Available online at www.sciencedirect.com
SCIENCE DIRECT®
Journal of Power Sources 123 (2003) 206–215
JOURNAL OF POWER SOURCES
www.elsevier.com/locate/jpowsour

Evolution of local electronic and atomic structure of Co-doped $LiMn_2O_4$ cathode material for lithium rechargeable batteries

B.J. Hwang [a,*], Y.W. Tsai [a], R. Santhanam [a], Y.W. Wu [a], S.G. Hu [a], J.F. Lee [b], D.G. Liu [b]

[a] *Microelectrochemistry Laboratory, Department of Chemical Engineering, National Taiwan University of Science and Technology, 43, Keelung Road, Sec. 4, Taipei 106, Taiwan, ROC*

[b] *Synchrotron Radiation Research Center, 1, R&D Road VI, Hsinchu Science-Based Industrial Park, Hsinchu 300, Taiwan, ROC*

Received 7 March 2003; accepted 24 March 2003

Abstract

In situ X-ray absorption spectroscopy (XAS) techniques are performed to investigate the evolution of the local electronic and atomic structure of a spinel cathode material $LiCo_{0.2}Mn_{1.8}O_4$ in the 4 V range. Changes in the oxidation state, bond distance, and local disorder of Mn and Co absorbers in the Co-doped $LiMn_2O_4$ are measured as a function of potentials. The X-ray absorption near edge spectra shows that charging (Li deintercalation) leads to the oxidation of manganese to Mn^{4+}. On the other hand, Co atoms are also oxidized but the edge energy shift is small, which suggests that Co is also electroactive in $LiCo_{0.2}Mn_{1.8}O_4$ in the 4 V range. The change in the Debye–Waller factor of the Co–O shell is smaller than that of Mn–O shell. Furthermore, from Debye–Waller factor and bond distance values, it appears that the Co environment fluctuates markedly during discharging.

Keywords: Electronic structure; Atomic structure XAS; Co-doped; $LiMn_2O_4$

1. Introduction

Spinel $LiMn_2O_4$ has been studied extensively as the potential candidate material for cathodes in lithium-ion rechargeable batteries due to its low cost and acceptable environmental characteristics [1–6]. Despite these advantages, however, $LiMn_2O_4$ exhibits high capacity fading on cycling because of the strong Jahn–Teller distortion of trivalent Mn. Hence, improvement in its electrochemical performance is essential for enhancing capacity retention by substituting Mn with other metal ions which may stabilize the spinel structure with or without participating in the redox processes [7–12]. The improvement of cycling stability observed when Mn^{3+} is substituted by other cations, such as Al^{3+}, Co^{3+}, Ni^{3+}, etc. can be attributed to a decrease in the local distortion of the lattice by Jahn–Teller active Mn^{3+} ions. Recently, we have undertaken detailed in situ X-ray absorption spectroscopy studies on nano-sized $LiAl_{0.15}Mn_{1.85}O_4$ cathode material in aqueous solution [13]. It was found that the ordering of Mn–O_6 octahedra is due mainly to the contribution from Mn–O (4) bonds. We have also demonstrated a method for the formation of $LCo_xMn_{2-x}O_4$ solid solution on the surface of the $LiMn_2O_4$. The $LiCo_xMn_{2-x}O_4$ material thus formed greatly enhanced the initial capacity, capacity retention and rate capability of the $LiCo_xMn_{2-x}O_4$ in the 4 V range [14]. The phase transformation of $LiMn_2O_4$ at room temperature can be also avoided by partial substitution of Mn^{3+} ions by Co^{3+} ions [15]. Furthermore, Kawai et al. reported reversible lithium extraction at ca. 5.1 V in Co-substituted $LiMn_2O_4$ [16]. This has been associated with the presence of Co^{3+} in the octahedral 16d positions of the spinel structure, and due to the $Co^{3+} \Leftrightarrow Co^{4+}$ redox processes [17–20]. All these reports indicate that Co in Co-substituted $LiMn_2O_4$ is active in the 5 V range but only plays a role of a stabilizer in the 4 V range. Nevertheless, Co seems to be the dopant that yields cathode materials with the highest reversible capacity in 4 V region [21].

It would be interesting to understand the local environment changes of Co-doped $LiMn_2O_4$ during charging and discharging processes. In this study a deep insight is provided into the local and electronic structure around a selected absorbing atom, viz., Co or Mn, in Co-doped $LiMn_2O_4$ cathode material by using in situ X-ray absorption spectroscopic measurements in the 4 V range during charging–discharging processes.

* Corresponding author. Tel.: +886-2273-76624; fax: +886-2273-76624.
E-mail address: bjh@ch.ntust.edu.tw (B.J. Hwang).

0378-7753/$ – see front matter © 2003 Elsevier Science B.V. All rights reserved.
doi:10.1016/S0378-7753(03)00516-0

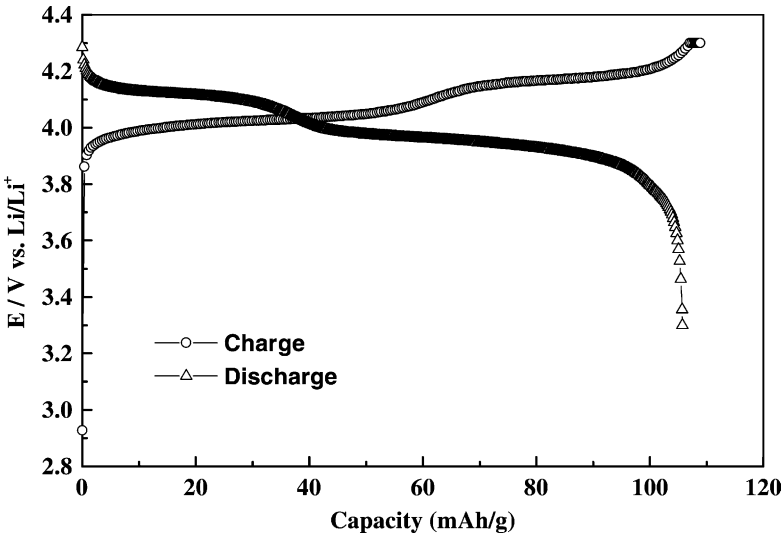

Fig. 1. Charge and discharge curves of $Li/LiCo_{0.2}Mn_{1.8}O_4$ cell from 3.3 to 4.3 V (charge rate: 0.2 C, discharge rate: 0.1 C).

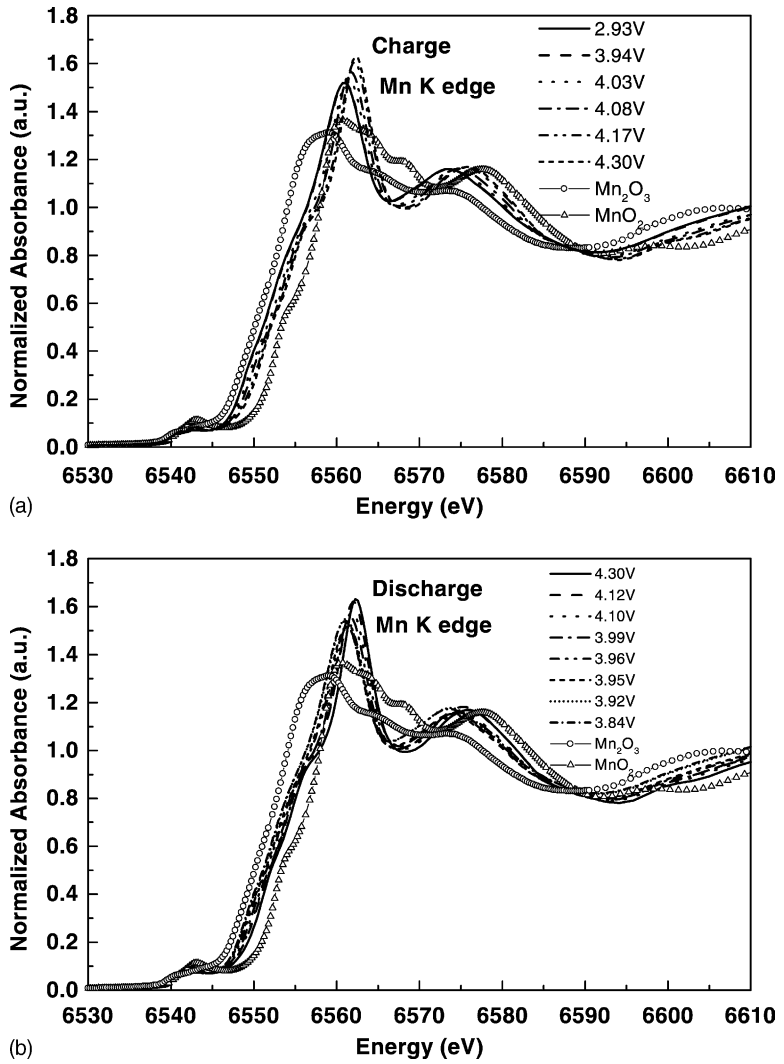

Fig. 2. K-edge XANES spectra for Mn in $LiCo_{0.2}Mn_{1.8}O_4$ at: (a) various charging potentials; (b) various discharging potentials. The spectrum is compared with those for Mn_2O_3 and MnO_2.

2. Experimental

$LiCO_{0.2}Mn_{1.8}O_4$ powders were synthesized by the sol–gel method using citric acid as a chelating agent [5,6]. A stoichiometric amount of lithium acetate ($Li(CH_3COO)\cdot 2H_2O$), cobalt nitrate ($Co(NO_3)_2\cdot 6H_2O$) and manganese acetate ($Mn(CH_3COO)_2\cdot 4H_2O$) was dissolved in distilled water and mixed with an aqueous solution of citric acid. The resulting solution was mixed with a magnetic stirrer at 80–90 °C for 5–6 h to obtain a clear viscous gel. The gel was dried in a vacuum oven at 140 °C for 24 h. The $LCo_{0.2}Mn_{1.8}O_4$ compounds were ground and calcined at 750–900 °C after precalcining the obtained precursor at 450 °C. During heating and cooling, the variation of temperature was fixed at 2 °C/min.

Electrochemical characterization was carried out with coin—type cells. The cathode was prepared by mixing a 85:3.5:1.5:10 (w/w) ratio of active material, carbon black, KS6 graphite and polyvinylidene fluoride binder, respectively, in *N*-methyl pyrrolidinone. The resulting paste was applied to a aluminum current-collector. The entire assembly was dried under vacuum overnight and then heated in an oven at 120 °C for 2 h. Lithium metal (FMC) was used as an anode and a polypropylene separator was used to separate anode and the cathode. 1.0 M $LiPF_6$ dissolved in a 1:1 mixture of ethylene carbonate (EC)/diethyl carbonate (DEC) was used as an electrolyte. The cells were assembled in an argon-filled dry box where both the moisture and the oxygen content were <1 ppm. Charge and discharge cycles were performed at the 0.1 C-rate over a potential range between 3.3 and 4.3 V.

In situ XAS experiments were carried out in transmission mode and florescence mode for Mn and Co K-edges, respectively, at the beam line BL-17C of the Synchrotron Radiation Research Center (SRRC) at Hsinchu, Taiwan. The storage ring was operated with an electron energy of 1.5 GeV and a current between 100 and 200 mA. A Si(1 1 1) double-crystal monochromator was employed for energy

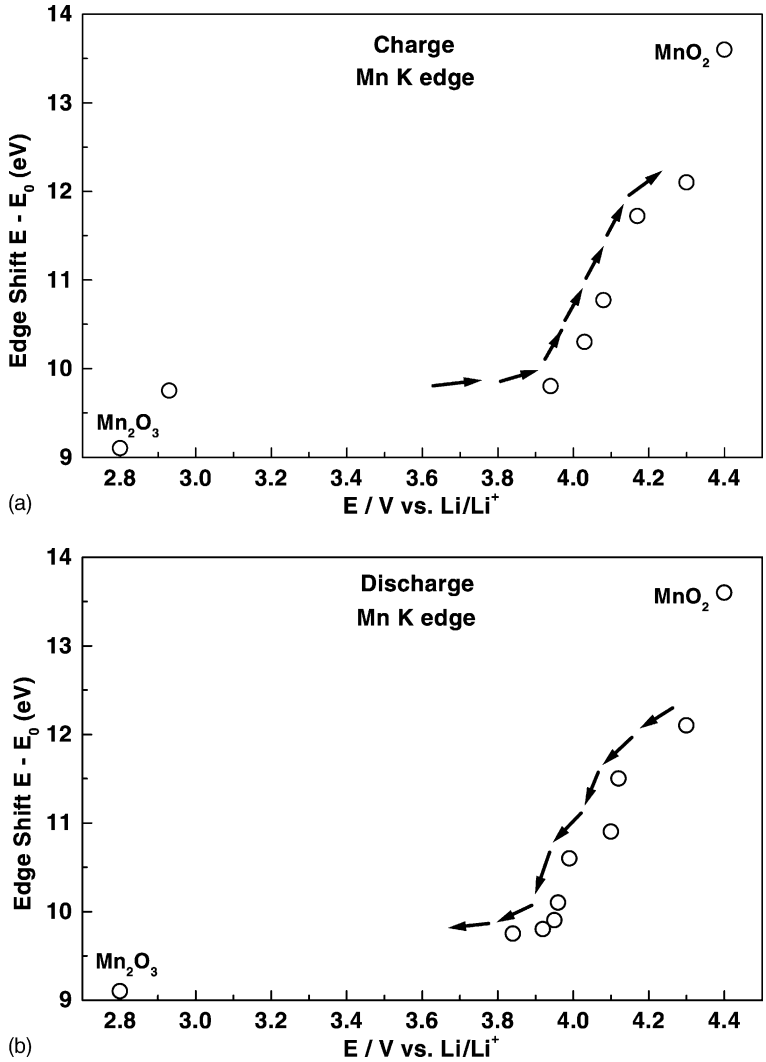

Fig. 3. Variation of Mn K-edge energy shift of $LiCo_{0.2}Mn_{1.8}O_4$ material at: (a) various charging potentials; (b) various discharging potentials. The energy shift is compared with the energy for Mn_2O_3 and MnO_2.

selection. High-order harmonic contamination was rejected by mirrors. Energy calibration was performed in each scan using a reference Mn foil or Co foil and was measured simultaneously.

Standard procedures were followed to analyze the EXAFS data. First, the raw absorption spectrum in the pre-edge region was fitted to a straight line and the background above the edge was fitted with a cubic spline. The EXAFS function, χ, was obtained by subtracting the post-edge background from the overall absorption and then normalized with respect to the edge jump step. The normalized $\chi(E)$ was transformed from energy space to k space, where k is the photoelectron wave vector. The $\chi(k)$ data were multiplied by k^3 to compensate the damping of EXAFS oscillations in the high-k region. Subsequently, k^3 weighted $\chi(k)$ data in the k-space ranging from 2.41 to 12.96 $Å^{-1}$ was Fourier transformed (FT) to r-space in order to separate the EXAFS contributions from different coordination shells. A non-linear least-squares algorithm was applied for curve fitting of EXAFS in r-space between 0.84 and 3.06 Å. All the computer programs were implemented in the UWXAFS 3.0 package with the backscattering amplitude and the phase shift for specific atom pair theoretically calculated by using FEFF7 code. The amplitude reduction factor S_0^2 was scaled to fixed values of 0.667 for Mn and 0.746 for Co, respectively, after refinements. The coordination numbers (N) were also fixed to the crystallographic values since the N value is highly correlated with the Debye–Waller factor. (Note that the coordination number of the first shell Mn–O/Co–O as well as second shell Mn–M/Co–M was fixed as 6).

3. Results and discussion

The charging and discharging curves of $Li/LCo_{0.2}Mn_{1.8}O_4$ from 3.3 to 4.3 V at 0.2 and 0.1 C, respectively, are shown

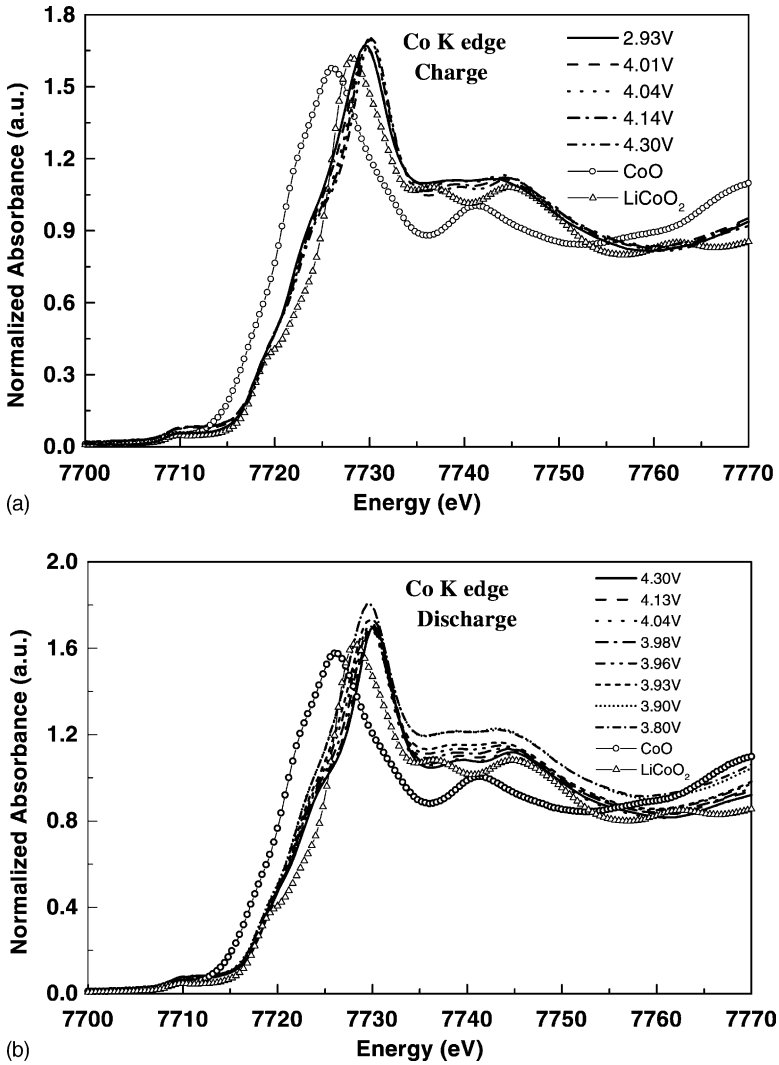

Fig. 4. K-edge XANES spectra for Co in $LiCo_{0.2}Mn_{1.8}O_4$ at: (a) various charging potentials; (b) various discharging potentials. The spectrum is compared with the spectra for CoO and $LiCoO_2$.

in Fig. 1. During charge, six and five scans were collected at the Mn and the Co edge, respectively, and during discharge eight scans were continuously collected at both the Mn and the Co edges, as indicated in Fig. 1. The charging and discharging capacities are 110 and 107 mAh g^{-1}, respectively. The Mn K-XANES spectra of $LiCo_{0.2}Mn_{1.8}O_4$ spinel material during charging (Li intercalation) and discharging (Li de-intercalation) as a function of potential are shown in Fig. 2a and b, respectively, with reference spectra of Mn_2O_3 and MnO_2 where the valence states of Mn are 3+ and 4+, respectively. It is known that the shift in edge energy position corresponding to an average oxidation state of a particular atom. The energy shift versus potential plot of $LiCo_{0.2}Mn_{1.8}O_4$ spinel at the Mn K-edge during charging and discharging is shown in Fig. 3a and b, respectively. The edge energies of the $LiCO_{0.2}Mn_{1.8}O_4$ are found to be lower than those of the Mn^{4+} reference, but higher than those of Mn^{3+} during both charging and discharging process. This observation indicates that there is a mixed oxidation state of manganese (Mn^{3+}/Mn^{4+}) in the $LiCo_{0.2}Mn_{1.8}O_4$ compound. It is also found that the edge energy is increased as the potential is increased from 2.93 to 4.30 V (charge) and is decreased as the potential is decreased from 4.30 to 3.84 V (discharge). This suggests an increase/decrease in the manganese oxidation state with increasing/decreasing potentials, respectively. From these results, obtained from XANES, it can concluded that the Li intercalation/de-intercalation process is reversible and that manganese ions are in the mixed valence state (Mn^{3+}/Mn^{4+}) in $LiCo_{0.2}Mn_{1.8}O_4$ during the charging and discharging processes. The change of edge shift between fully charged and fully discharged is around 2.5 eV.

The Co K-XANES spectra of $LiCo_{0.2}Mn_{1.8}O_4$ spinel during charging and discharging as a function of potential are shown in Fig. 4a and b, respectively, with reference spectra of CoO and $LiCoO_2$ where the valence states of Co are 2^+

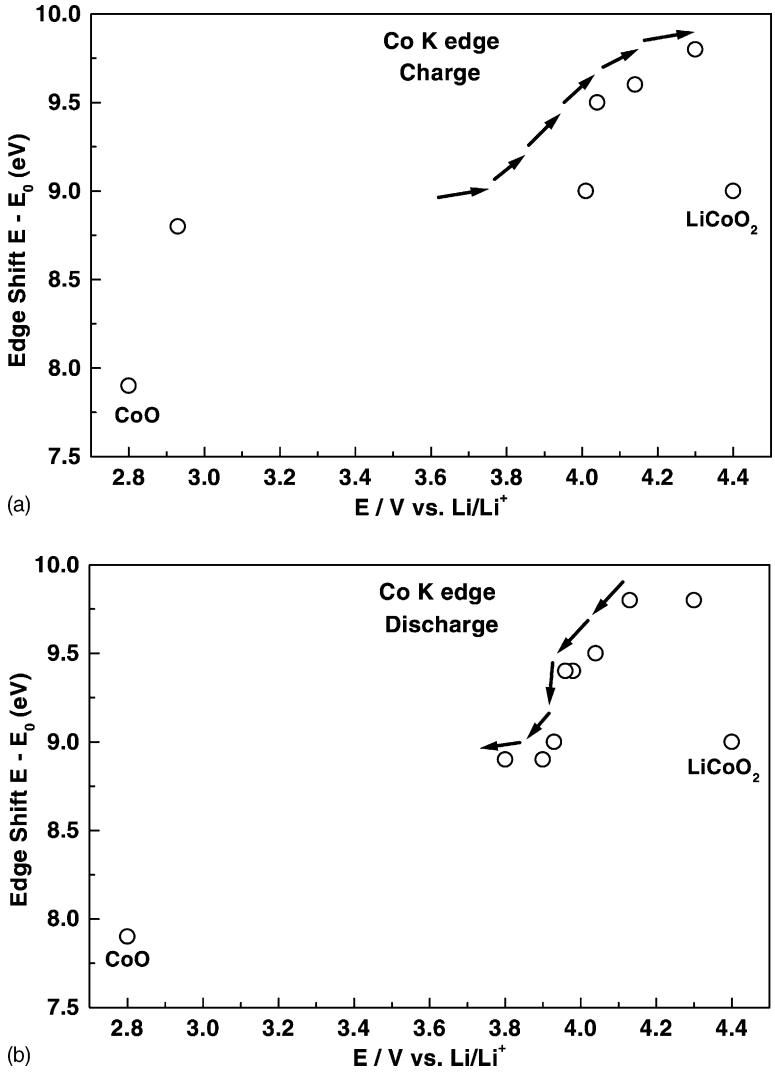

Fig. 5. Variation of Co K-edge energy shift of $LiCo_{0.2}Mn_{1.8}O_4$ material at: (a) various charging potentials; (b) various discharging potentials. The energy shift is compared with the energy for CoO and $LiCoO_2$.

and 3^+, respectively. The energy shift versus potential plot of $LiCO_{0.2}Mn_{1.9}O_4$ spinel at the Co K-edge during charging and discharging are presented in Fig. 5a and b, respectively. The edge energies of the $LiCo_{0.2}Mn_{1.8}O_4$ are higher than those of the Co^{3+} reference around the 4 V range during both charging and discharging processes. Several reports have demonstrated that Co^{3+} is electroactive only in the 5 V range [17–20]. From the present results, however, it appears that Co oxidizes/reduces during charging/discharging. As can be seen in Fig. 5a and b, Co^{3+} oxidizes in the 4 V range during charging and reduces during discharging as a function of potential, but the energy shift of the Co K-edge is smaller than that of the Mn K-edge, which suggests that Co^{3+} ions play the role of active materials in Co-doped $LiMn_2O_4$. This may explain the fact that Co-doped $LiMn_2O_4$ has been reported to give higher capacity (relevant to higher capacity in the 4 V region) [21].The Fourier Transforms of Mn and Co in $LiCo_{0.2}Mn_{1.8}O_4$ spinel are given in Figs. 5–7, respectively, as a function of charging as well as discharging potential. The first peak at ~1.5 Å in Fig. 6a and b and in Fig. 7a and b, is due to Mn–O and Co–O interaction, respectively. As the sample is charged (de-intercalation), it can be seen that the amplitude of the Mn–O peak increases while that of the Co–O peak remains almost constant. The increase in amplitude is ascribed to changes in the local structure of Mn created by the oxidation of Mn^{3+} to Mn^{4+}. Since Mn^{4+} is not a Jahn–Teller active ion, oxidation of Mn^{3+} to Mn^{4+} results in a decrease of the Jahn–Teller effect and gives rise to an increase in the amplitude of the Mn–O peak. As the Co^{3+} is not a Jahn–Teller active ion, no change in the amplitude of the Co–O peak is observed. Almost reversible changes in amplitude are observed during discharge in the case of Mn–O interactions. In the case of Co–O interactions, however, some irregular changes are observed. This result indicates that the Co environment appears to be complicated during lithium intercalation (discharging) into $LiCo_{0.2}Mn_{1.8}O_4$ spinel material. The second peak at ~2.5 Å in Figs. 6a,b and 7a,b corresponds to a metal–metal interaction. It

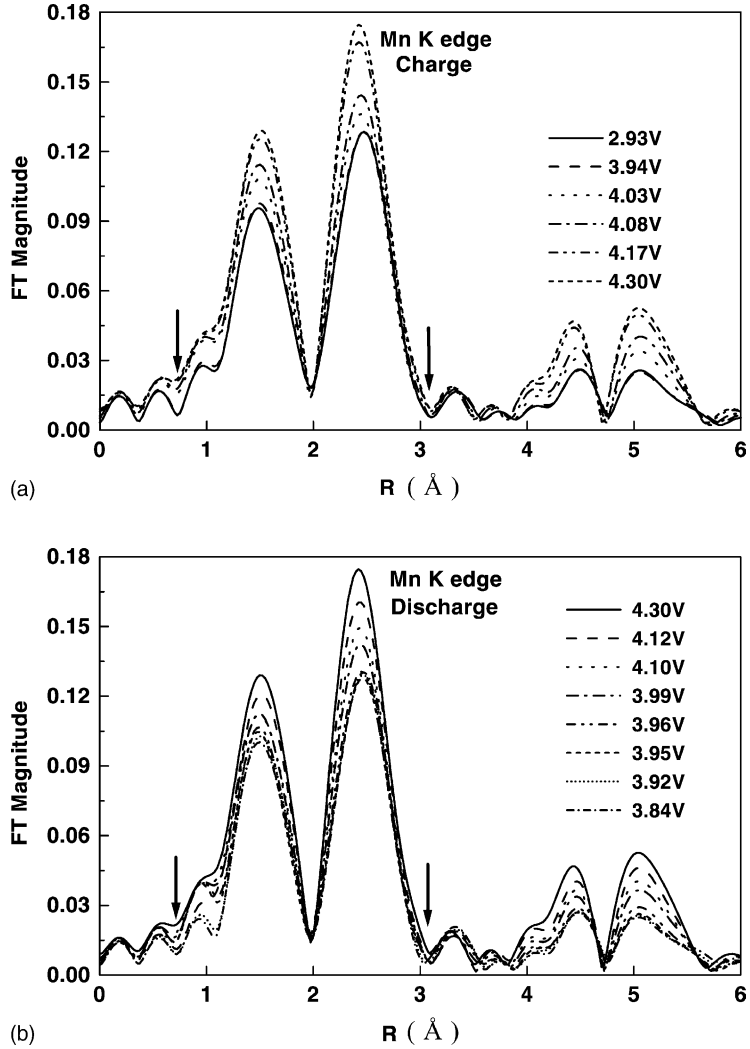

Fig. 6. Fourier transform spectra for Mn in $LiCo_{0.2}Mn_{1.8}O_4$ at: (a) various charging potentials; (b) various discharging potentials.

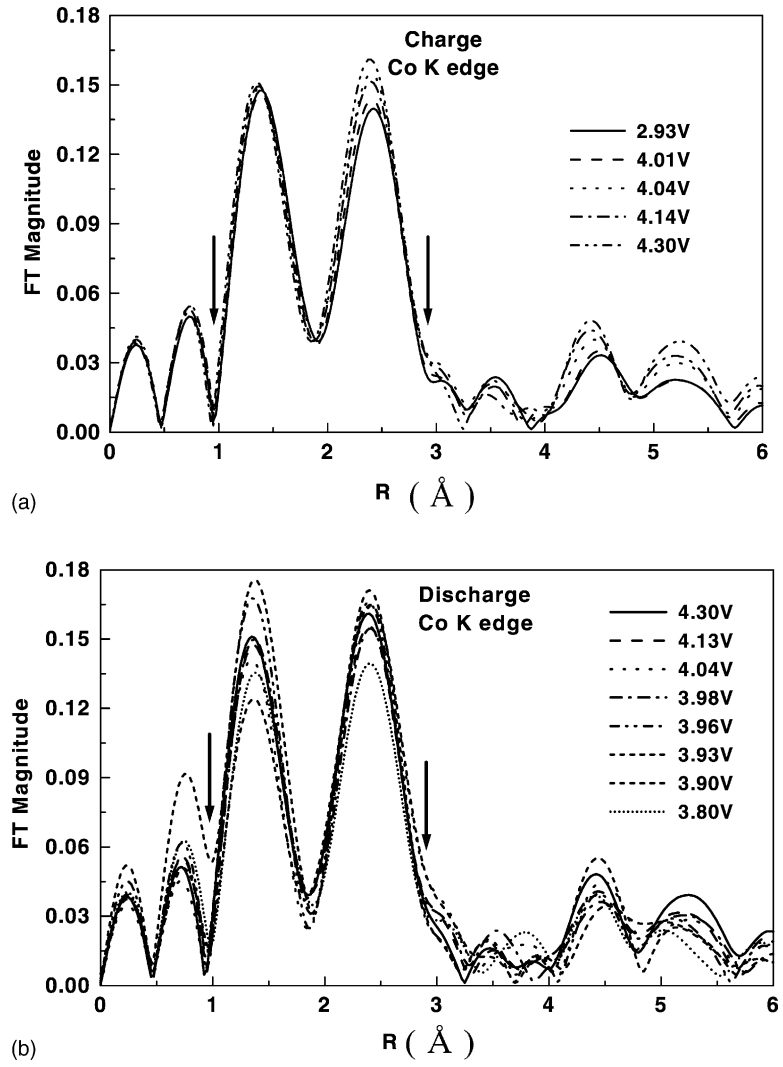

Fig. 7. Fourier transform spectra for Co in $LiCo_{0.2}Mn_{1.8}O_4$ at: (a) various charging potentials; (b) various discharging potentials.

is found that at both the Mn and Co edges the peak position shifts to lower *r* values and also increases in amplitude during charging. These features are reversible during discharging.

Curve-fitting analysis has been carried out in order to determine the structural parameters of $LiCo_{0.2}Mn_{1.8}O_4$ cathode material such as bond distance (*R*), Debye–Waller factor (σ^2) for the first shell M–O and the second shell M–M. The curve-fitting analysis for the first two Fourier transform peaks was done by two-shell model. In this model, all six M–O bonds in the MO_6 octahedron are considered to be the same. In order to observe the changes clearly, fitted parameters such as bond distance (*R*), Debye–Waller factor (σ^2) for the 1st shell M–O and the 2nd shell M–M of $LiCo_{0.2}Mn_{1.8}O_4$ are plotted against potential during lithium de-intercalation and intercalation as shown in Fig. 8. At the Mn K-edge, the first shell Mn–O (Fig. 8a) as well as the second shell Mn–M (Fig. 8b) bond distances determined from EXAFS decrease and then increase during lithium de-intercalation and intercalation, respectively. The Debye–Waller factor of Mn–O decreases from 0.0071 to 0.0039 $Å^2$ and increases to 0.0065 $Å^2$ while that of Mn–M decreases from 0.0065 to 0.0046 $Å^2$ and increases to 0.0064 $Å^2$ during charging and discharging, respectively (Fig. 8c and d). Thus, the change in the Debye–Waller factor of the Mn–O shell is greater than that of the Mn–M shell. The variation in bond distance and the Debye–Waller factor are shown in Fig. 9 at various charging and discharging potentials for the first shell Co-O and the second shell Co–M at the Co–K-edge of $LiCo_{0.2}Mn_{1.8}O_4$. During charging, for both the shells, the bond distance and the Debye–Waller factors decrease consistently (Fig. 9a and b). During discharging, however, the changes in these values are inconsistent (Fig. 9c and d). This result indicates that the Co environment is complicated during the lithium intercalation process.

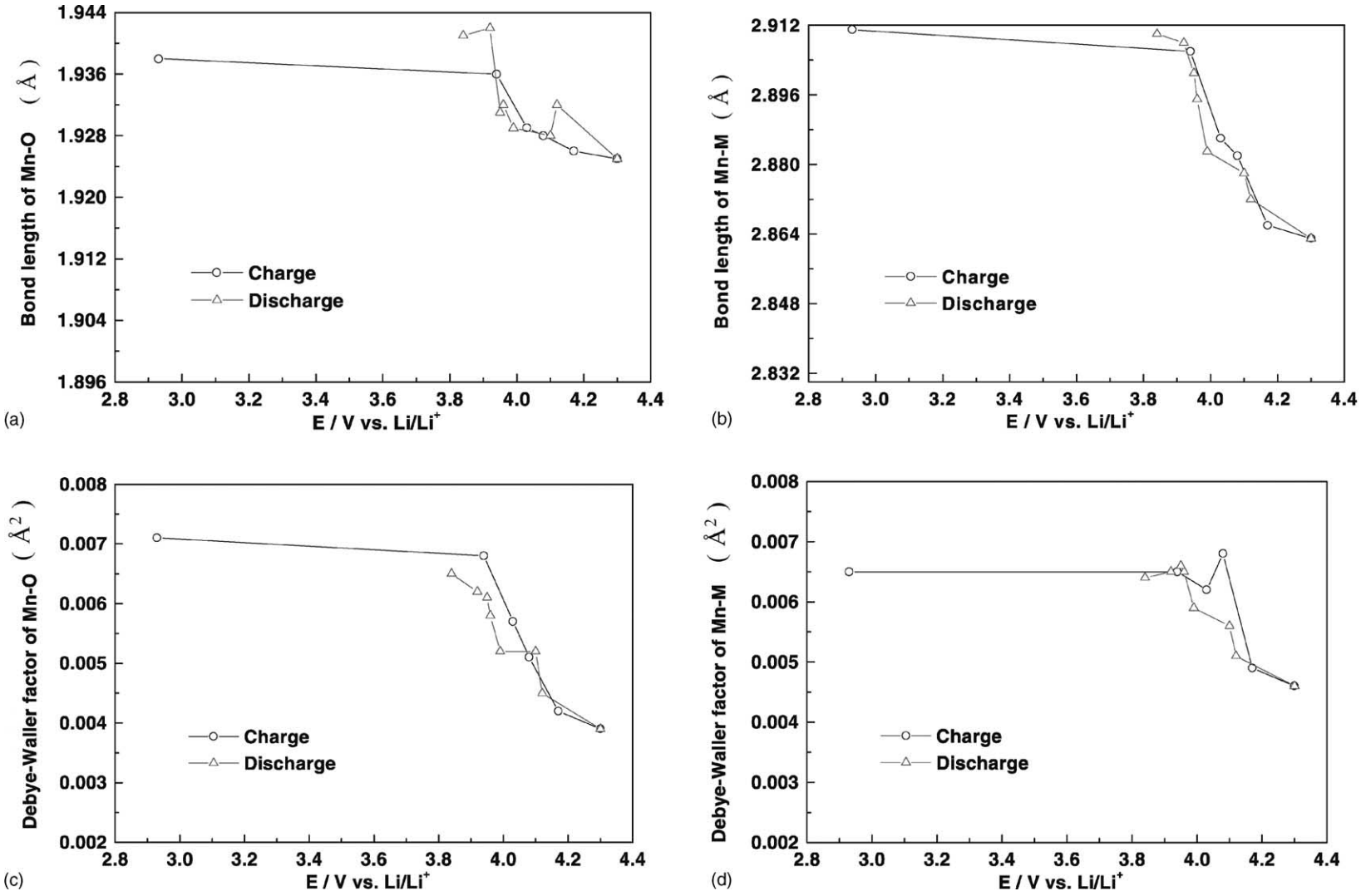

Fig. 8. Variation of bond distances (a) Mn–O; (b) Mn–M and Debye–Waller factors; (c) Mn–O; (d) Mn–M in $LiCo_{0.2}Mn_{1.8}O_4$ at various charging and discharging potentials.

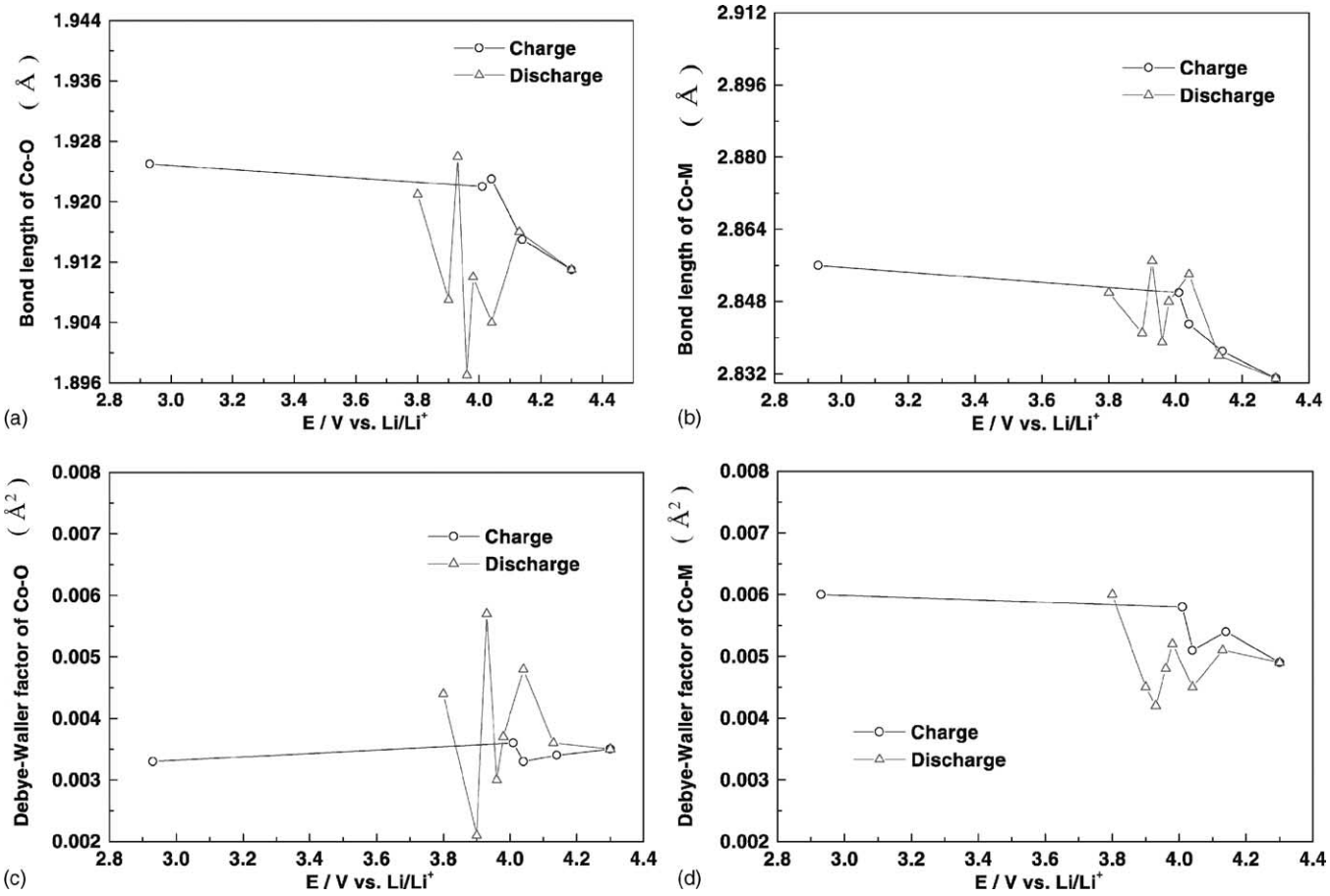

Fig. 9. Variation of bond distances (a) Co–O; (b) Co–M and Debye–Waller factors; (c) Co–O; (d) Co–M in $LiCo_{0.2}Mn_{1.8}O_4$ at various charging and discharging potentials.

4. Conclusions

The evolution the local electronic and atomic structure of $LiCo_{0.2}Mn_{1.8}O_4$ cathode material has been in investigated by means of Mn and Co K-edge XAS measurements during charging and discharging. Changes in the bond distances and the local disorder have been measured as a function of potential. The change in the oxidation states of Mn and Co are observed from XANES during the charging and the discharging process in the 4 V range. It reveals that Co in the Co-substituted $LiMn_2O_4$ is electroactive in the 4 V range. The bond distances and Debye–Waller factors decreases and increase consistently during the charging and the discharging processes. During discharging, however, inconsistent changes are observed in bond distances and Debye–Waller factors. This observation indicates that the Co environment is complicated during the discharge process.

Acknowledgements

Financial support from the National Science Council (NSC 89-2214-E-011-044 & NSC 90-2811-E-0110055), the Education Ministry (EX-91-E-FA09-5-4), the Synchrotron Radiation Research Center (SRRC), Hsinchu, and the National Taiwan University of Science and Technology, Taiwan, Republic of China is gratefully acknowledged.

References

[1] M.M. Thackeray, J. Am. Ceram. Soc. 82 (1999) 3347.
[2] D. Guyomard, J.M. Tarascon, Solid State Ionics 69 (1994) 222.
[3] D. Guyomard, J.M. Tarascon, J. Electrochem. Soc. 139 (1992) 937.
[4] M.M. Thackeray, Prog. Solid State Chem. 25 (1997) 1.
[5] B.J. Hwang, R. Santhanarn, D.G. Liu, J. Power Sources 97–98 (2001) 443.
[6] B.J. Hwang, R. Santhanam, D.G. Liu, J. Power Sources 101 (2001) 86.
[7] J.H. Lee, J.K. Hong, D.H. Jang, Y.K. Sun, S.M. Oh, J. Power Sources 89 (2000) 7.
[8] J.M. Amarilla, J.L. Martin de Vidales, R.M. Rojas, Solid State Ionics 127 (2000) 73.
[9] Y.S. Lee, M. Yoshio, Electrochem. Solid State Lett. 4 (2001) A155.

[10] H. Shigemura, M. Tabuchi, H. Kobayashi, H. Sakaebe, A. Hirano, H. Kageyama, J. Mat. Chem. 12 (2002) 1882.
[11] B.J. Hwang, R. Santhanam, D.G. Liu, Y.W. Tsai, J. Power Sources 102 (2001) 326.
[12] B.J. Hwang, R. Santhanam, S.G. Hu, J. Power Sources 108 (2002) 250.
[13] B.J. Hwang, R. Santhanam, C.P. Huang, Y.W. Tsai, J.F. Lee, J. Electrochem. Soc. 149 (2002) A694.
[14] B.J. Hwang, Y.W. Tsai, R. Santhanam, D.G. Liu, J.F. Lee, J. Electrochem. Soc. 150 (2003) A335.
[15] C.H. Chen, R.S. Liu, R. Gundakaram, J.M. Chen, S.M. Huang, J.S. Chen, C.M. Wang, J. Power Sources 102 (2001) 21.
[16] H. Kawai, M. Nagata, H. Tukamoto, A.R. West, J. Mater. Chem. 8 (1998) 837.
[17] H. Kawai, M. Nagata, H. Tukamoto, A.R. West, Electrochem. Solid State Lett. 1 (1998) 212.
[18] H. Kawai, M. Nagata, H. Tukamoto, A.R. West, Electrochim. Acta 45 (1999) 315.
[19] P. Aitchison, B. Ammundsen, D.J. Jones, G. Burns, J. Roziere, J. Mat. Chem. 9 (1999) 3125.
[20] S. Mandal, R.M. Rojas, J.M. Amarilla, P. Calle, N.V. Kosava, V.F. Anufrienko, J.M. Rojo, Chem. Mat. 14 (2002) 1598.
[21] L. Guohua, H. Ikuta, T. Uchida, M. Wakihara, J. Electrochem. Soc. 143 (1996) 178.